Proceedings of the ASME 2016 International Design Engineering Technical Conferences and Computers and Information in Engineering Conference
IDETC/CIE 2016
August 21-24, 2016, Charlotte, North Carolina

DETC2016-59412

SYNTHESIZING PLANAR RIGID-BODY CHAINS FOR MORPHOMETRIC APPLICATIONS

Bingjue Li* **Andrew P. Murray** **David H. Myszka**
Design of Innovative Machines Laboratory
Department of Mechanical & Aerospace Engineering
University of Dayton
Dayton, Ohio 45469
Email: lib002@udayton.edu

Gérard Subsol
Research-team ICAR
Laboratory of Informatics, Robotics and Microelectronics
CNRS/University of Montpellier, France

ABSTRACT

Morphometrics is a quantitative analysis to compare a set of geometric representations of forms, including shape and size. Analysis of shape variation is useful in systematics, evolutionary biology, biostratigraphy, and developmental biology. Distinguished by the data being analyzed, three forms of morphometrics are commonly recognized. Traditional morphometrics measures the lengths, ratios, angles, etc., of patterns of shape variations. Outline-based morphometrics analyzes the outlines of forms using open or closed curves. Landmark-based geometric morphometrics summarizes shapes in terms of the coordinates of anatomical landmarks. The three morphometric methods are able to capture the variation of forms exactly, but require analyzing numerous variables. As an alternative approach to morphometrics, this paper presents a kinematic synthesis methodology of planar rigid-body chains. This methodology approximates the set of profile curves that represent a series of shapes with a single chain comprised of rigid-body links connected by revolute or prismatic joints. The primary advantage of the presented approach is that a modest number of physical parameters describes the shape and size change between a set of curves. Three morphometric problems are investigated by applying the methodology of synthesizing planar rigid-body chains to match the prescribed shapes. The result validates that the presented methodology might be used as an alternative approach to the analysis of morphological forms.

1 INTRODUCTION

Shape analysis has been an essential component of biology research. Morphometrics is the quantitative study of biologic shape, shape variation, and covariation with other variables or factors. Describing and comparing morphological shapes has provided fundamental information for taxonomic classification of organisms and understanding the diversity of biological life [1]. Based on the data being analyzed, forms of morphometrics are usually distinguished as traditional morphometrics, landmark-based geometric morphometrics, and outline-based geometric morphometrics. Traditional or multivariate morphometrics uses multivariate statistical tools to analyze a small set of variables which characterize the global shape as diameters or angles [2, 3]. Several difficulties remain in traditional morphometrics, such as choosing the most appropriate method for size correction, assessing a common definition of the variables among all the shapes, distinguishing small variations of the shapes which are not emphasized by the global variable, and generating graphical representations of shape variations from variables. Geometric morphometrics (including outline- and landmark-based methods) are now common methods of analyzing morphological shapes as they are able to capture the whole geometry of morphological structures and preserve this information throughout the analysis. Outline-based geometric morphometrics fits the coordinates of the points sampled from the outline of a structure or region with a mathematical function, typically in some form of

*Address all correspondence to this author.

Fourier analysis, and then analyzes the coefficients of the functions as multivariate parameters [4]. Major concerns about outline-based methods are that the sampling points do not have clear correspondences among specimens, and different fitting methods yield different results [5]. Landmark-based geometric morphometrics involves the analysis of collections of discrete biological landmarks. Each landmark is described by its two- or three-dimensional coordinates. The limitation of the landmark-based method is that non-shape variations (such as position, orientation, and scale of the specimen) cannot be analyzed directly and need to be mathematically eliminated prior to analysis. Additionally, comparing multiple complex shapes using geometric morphometrics requires a large number of landmarks, which increases the difficulty of the analysis.

This paper presents the methodology for synthesizing a rigid-body chain that can match a set of curves and shows the potential of applying it to two-dimensional (2D) morphometric problems. A shape matching problem starts with specifying a set of 2D curves (profiles) that describe the shapes of interest. For example, as shown in Fig. 1, the shape of a syrphidae (also known as flower fly) wing is described by a curve that connects 16 landmarks positioned at vein intersections or terminations [6]. Several curves would be collected in the same fashion from a number of syrphidae wing specimens. The goal of the synthesis is to design a jointed rigid-body chain to match each of the series of prescribed profiles with its edge geometries, allowing comparison of all shapes using one single chain. Analyzing the movements of the joints in the chain provides information about the variation and invariant of the shapes. Note that for morphometric and other shape-change problems that have been studied by the authors, the analysis focuses on the variation in profile shapes rather than the motion of the chain.

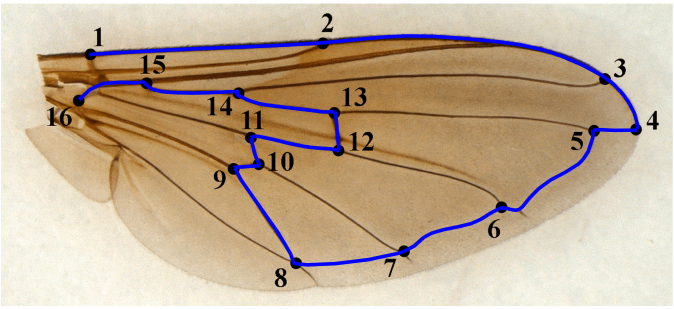

FIGURE 1. THE PROFILE OF A WING OF A SYRPHIDAE OBTAINED BY TRACING A CURVE ALONG 16 LANDMARKS.

The presented work is based on the methodology of synthesizing shape-changing rigid-body mechanisms, which approximates a series of shape variations with the edge geometry of a chain composed of rigid bodies connected by revolute joints and prismatic joints [7, 8]. Prismatic joints enable the rigid-body chain to approximate profiles with significant variation of arc length [9]. One limitation of these works is that the presence of revolute joints in the chain is mandatory, which could be unwanted in some cases. Fused connections are introduced to accommodate the need for eliminating or reducing the use of revolute joints, providing the capacity to achieve shape change via primarily prismatic joints [10].

The remainder of the paper is organized as follows. Section 2 summarizes the general procedure for synthesizing a rigid-body chain for shape matching. Section 3 presents the developments in the methodology, including matching profiles containing sharp corners, shifting endpoints for closed profiles to reduce matching error, and assembling the chain with revolute joints. In Sec. 4, the methodology is applied to three morphometric problems and results are presented.

2 SUMMARY OF METHODOLOGY FOR RIGID-BODY SHAPE CHANGE SYNTHESIS

The synthesis of rigid-body chains for shape matching includes two parts: target profile generation and segmentation. The synthesis initiates with a set of curves called design profiles, which represent the shapes of interest. As shown in Fig. 2, design profiles are categorized into open profiles [7], closed profiles [8], and profiles with endpoints fixed by revolute joints or prismatic joints [10, 11]. Most morphological curves fall into the open or closed type. Design profiles are converted to target profiles, which are piecewise linear curves with roughly equal piece lengths. Hence, the arc length of a design profile is quantified by the number of pieces in the corresponding target profile. In the segmentation process, the set of target profiles are approximated by a single chain of rigid bodies connected by revolute or prismatic joints, as shown in Fig. 3. Note that by varying the angles of the revolute joints and the lengths of the $\mathscr{C}$-segments, the chain varies its configuration to match the shapes of different profiles in the set. The geometry (shape and length) of the bodies are iteratively optimized until a chain that best matches the set of target profiles is obtained. In the presented work, the rigid-body chain is described by a number of segments and the connections between them. There are two types of segments, $\mathscr{M}$-segments and $\mathscr{C}$-segments. An $\mathscr{M}$-segment represents a rigid body that approximates a portion of the same number of pieces for all profiles. A $\mathscr{C}$-segment represents constant curvature links that contain a prismatic joint, and approximates a variable number of pieces on each target profile. The $\mathscr{C}$-segments enable the chain to match a set of profiles of significantly different arc lengths. Two segments can be connected by a revolute joint ($\mathscr{R}$) or fused ($\mathscr{F}$) at a fixed angle.

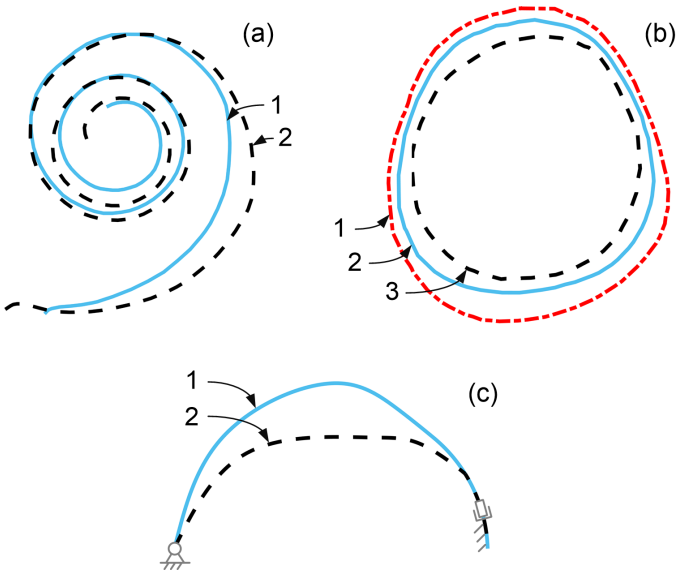

FIGURE 2. TYPES OF DESIGN PROFILES INCLUDE (a) OPEN PROFILES, (b) CLOSED PROFILES, AND (c) FIXED-END PROFILES.

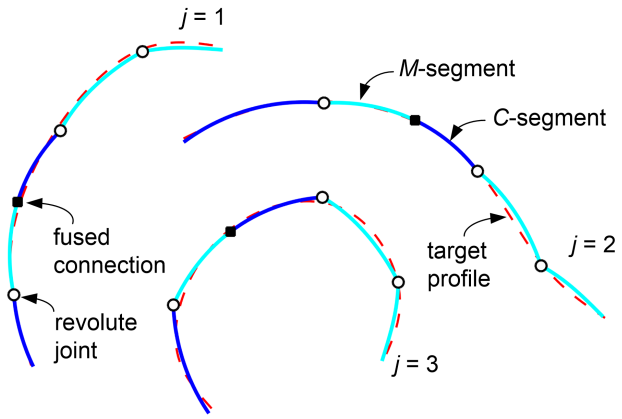

FIGURE 3. A RIGID-BODY CHAIN APPROXIMATES THE SHAPE OF THREE TARGET PROFILES.

2.1 Terminology for Rigid-Body Chain Synthesis

The flowchart shown in Fig. 4 illustrates the general procedure of the proposed synthesis methodology. The terminology used in this paper is consistent with Ref. [10]. First, a set of p design profiles are specified. Design profiles represent the desired shapes to be approximated by the rigid-body chain, and may be defined in various ways, such as curve functions, point coordinates, line drawings, etc. Each design profile is converted to a target profile by equally distributing N_j points along the design profile, where j is the profile number. Therefore the j^{th} target profile contains $N_j - 1$ linear pieces. For example, by specifying a minimum profile length of 2000 pieces, the three target profiles in Fig. 3 are generated containing 2000, 2322, and 2253 linear pieces with an average piece length of 0.0577. Piecewise linear target profiles are used in all following analyses, and are referred to as "profiles". Next, the analyst would specify an appropriate structure of the chain, including the number of segments (q), the type of segments (represented by the segment type vector, $\mathbf{V}$), and the type of connections between segments (represented by the connection type vector, $\mathbf{W}$). The chain shown in Fig. 3 has a segment type vector $\mathbf{V} = [\mathscr{C}\ \mathscr{M}\ \mathscr{C}\ \mathscr{M}\ \mathscr{M}]$ and a connection type vector $\mathbf{W} = [\mathscr{R}\ \mathscr{F}\ \mathscr{R}\ \mathscr{R}]$. Then, a population (usually several hundred) of segment matrices (SM) are randomly generated. An SM is a $p \times q$ matrix in which each entry m_j^e represents the number of pieces contained in the e^{th} segment for the j^{th} profile. Note that a column of SM corresponding to an $\mathscr{M}$-segment would have equal entries, as an $\mathscr{M}$-segment has the same number of pieces for all profiles.

After an SM is generated, segments are constructed accordingly. An $\mathscr{M}$-segment represents the average shape of the corresponding portions of profiles [7]. A $\mathscr{C}$-segment is created with the average curvature of all points on the corresponding portion of all profiles. The length of each piece in a $\mathscr{C}$-segment equals the average piece length of its corresponding portions of the target profiles [9]. Once generated, segments are shifted to align with the profiles such that the total error to match each profile is minimized, and the angles between them are measured. Then, the connections between segments, specified as $\mathscr{F}$ in the connection type vector $\mathbf{W}$, are fused at the average angle.

After being fused, segments are repositioned to align with the profiles again. A $p \times q$ error matrix (EM) is constructed to evaluate the matching error of each segment. Each component E_j^e is calculated as the maximum point-to-point matching error of the e^{th} segment at the j^{th} profile. For process efficiency, only a few (typically 1-5) SMs that yield the lowest average matching error are kept for optimization. The optimization uses a gradient-based iterative method to adjust SM, such that the matching error is minimized. Note that each time the matching error is evaluated, the segments are aligned with the profiles at their error-minimizing locations. Finally, the chain is constructed according to each final SM, and revolute joints are added to assemble all segments into a continuous chain.

There are two reasons for not adding revolute joints until the last step. First, experience shows that optimizing the chain without adding revolute joints in the iterative process does not have considerable impact on the final result. Second, the step of adding revolute joints consumes significant computation time relative to other steps. This is more so as the number of design profiles and the number of joints in the chain increases. Therefore, adding revolute joints is not favorable in the process of generating a large population of initial SMs or in the iterative optimization process. In summary, adding revolute joints in the

optimizing process does not effectively yield better results, but significantly increases the computation time, therefore revolute joints are not added until the chain has been optimized.

For the chain shown in Fig. 3, the optimized *SM* is

$$SM = \begin{bmatrix} 326\ 420\ 376\ 522\ 356 \\ 660\ 420\ 364\ 522\ 356 \\ 509\ 420\ 446\ 522\ 356 \end{bmatrix}.$$

Note that the the entries in the 2nd, 4th, and 5th columns have the same values because they correspond to $\mathscr{M}$-segments, and that the sum of each row equals the total number of pieces in each target profile.

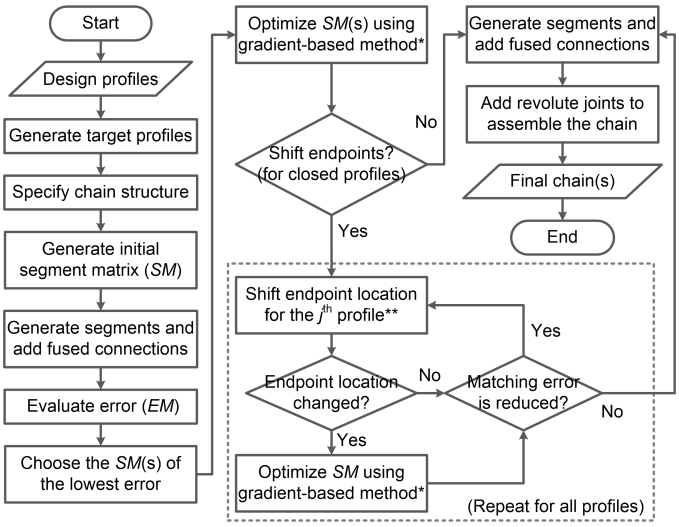

FIGURE 4. THE FLOWCHART OF GENERAL PROCEDURES IN RIGID-BODY CHAIN SYNTHESIS. SEE FIGS. 5 AND 8 FOR MORE DETAILS ON STEPS * AND **.

2.2 Optimization of the Segment Matrix

Figure 5 presents the gradient-based method for optimizing the *SM*. During each step of the iteration, the segments are generated according to the segment type vector **V** and the segment matrix *SM*, some connections are fused according to the connection type vector **W**, and the error matrix *EM* is constructed. The *SM* is adjusted according to the *EM* such that segments that have higher error are shortened while segments of lower error are elongated. The error of the e^{th} $\mathscr{C}$-segment on profile j is E_j^e. Evaluation of an $\mathscr{M}$-segment is based on the average matching error over all profiles defined as

$$\bar{E}^e = \frac{1}{p}\sum_{j=1}^{p} E_j^e, \tag{1}$$

where e is the segment number in the chain. The detailed method of evaluating and adjusting the *SM* according to the *EM* can be found in Ref. [10]. The overall matching error of an *SM* is defined as the average value of the *EM*, which is

$$\bar{E} = \frac{1}{pq}\sum_{j=1}^{p}\sum_{e=1}^{q} E_j^e. \tag{2}$$

This process is repeated until $\bar{E}$ has not decreased during the prior 10 steps. The *SM* that yields the lowest $\bar{E}$ is recognized as the result of the optimization.

Note that there is a random factor in selecting the order of adjusting the segments, therefore the same initial *SM* may be optimized to different results. Many local minima commonly exist in the solution field.

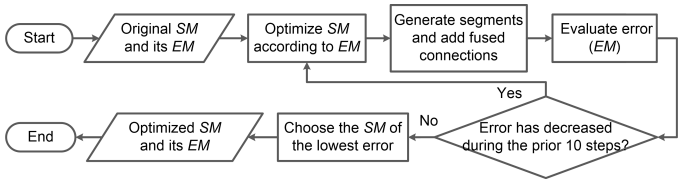

FIGURE 5. THE GRADIENT-BASED METHOD FOR OPTIMIZING A GIVEN *SM* USED IN THE STEP MARKED BY '*' IN FIG. 4.

3 DEVELOPMENTS OF METHODOLOGY FOR MORPHOMETRICS

In this section, developments of the rigid-body chain methodology for morphometrics are presented. First, methods for matching profiles that contain sharp corners are given. Second, shifting endpoints for closed profiles to potentially improve shape matching is presented. Third, a method for assembling the chain with revolute joints is presented.

3.1 Profiles Containing Sharp Corners

In morphometric problems, many curves have sharp corners or high curvature regions such as landmarks 4, 5, 8-13 of the profile curve of the syrphidae wing shown in Fig. 1. Recall that a $\mathscr{C}$-segment serves the purpose of allowing the chain to match a set of profiles of different arc lengths, and is obtained

using the average curvature of the corresponding portions. Using a $\mathscr{C}$-segment to match the sharp corner region generates a bad result because the average curvature is greatly affected by the sharp corner (the current optimization algorithm does not prevent a $\mathscr{C}$-segment from including a sharp corner). Avoiding $\mathscr{C}$-segments that include sharp corners can be done by adding a few constraints in the optimization process. A judicious choice is to approximate the sharp corner region with two $\mathscr{M}$-segments connected by a revolute joint (since an $\mathscr{M}$-segment matches the shapes better than a $\mathscr{C}$-segment does, and $\mathscr{C}$-segments are problematic around sharp corner regions). The sharp corner region can also be approximated by a single $\mathscr{M}$-segment, if the corresponding portions on all target profiles have roughly equal angle.

Consider the example shown in Fig. 6a, where each of the two fixed-end profiles contains a sharp corner. A chain of three $\mathscr{C}$-segments is used to match the two profiles with the segment matrix

$$SM = \begin{bmatrix} 608 & 112 & 680 \\ 390 & 181 & 833 \end{bmatrix}.$$

The shape of the sharp corner region on Profile 2 is poorly matched by the second $\mathscr{C}$-segment. Note that the other segments approximate the shape of their corresponding portions properly. After being assembled, the other segments are shifted from the original error-minimizing positions and consequently the matching error is increased significantly. As a result, the prior gradient-based method does not shorten the $\mathscr{C}$-segment that approximates the region with the sharp corner, and may even elongate it as other segments now have higher error.

When sharp corners exist, they should be evaluated and located. The curvature of a piecewise linear target profile at point i is defined as the reciprocal of the circumradius of the points $i-1$, i, and $i+1$. As shown in Fig. 7, the sharp corner of a design profile is not always represented accurately by the piecewise linear target profile. The curvature values at the two points adjacent to the sharp corner do not converge as the number of pieces in the target profile increases, and cannot be used to measure the angle of the sharp corner. Note that the angle between the two pieces adjacent to the sharp corner converges as the target profile contains a sufficient number of pieces. Therefore, the angle change between the $(i-1)^{\text{th}}$ and the $(i+1)^{\text{th}}$ pieces is measured and termed as the "bend angle" at the i^{th} piece. The bend angle is a signed value: a positive value indicates the curve bends counterclockwise, and vice versa. The bend angle of a sharp corner would be much higher than a smooth curve, thus it can be used to quantify and identify sharp corners. Once a sharp corner is identified, an apices matrix A_j is constructed for the j^{th} profile, with each column recording the location and bend angle of the sharp corners (or high-curvature regions) on that profile. The points on target profiles where the sharp corners occur are

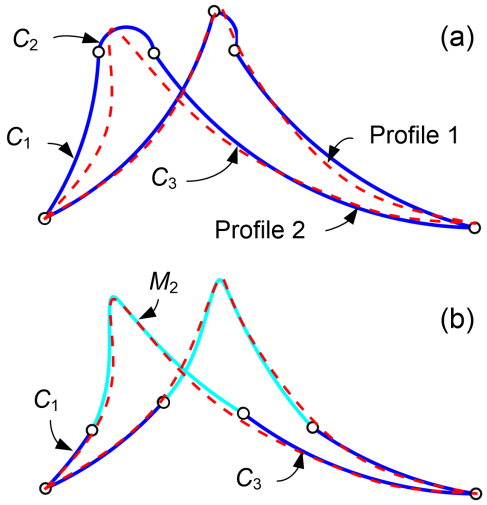

FIGURE 6. APPROXIMATE PROFILES CONTAINING HIGH-CURVATURE REGIONS WITH (a) THREE $\mathscr{C}$-SEGMENTS AND, (b) TWO $\mathscr{C}$-SEGMENTS AND AN $\mathscr{M}$-SEGMENT.

considered to be inviolable for $\mathscr{C}$-segments, meaning that $\mathscr{C}$-segments are not allowed to contain these points. At each step during the optimization, the SM is checked against the apices matrices to ensure that the inviolable points are not included in any $\mathscr{C}$-segments, otherwise the SM is reset to the previous value (note that the SM could continue to be optimized as there is a random factor in the optimization process).

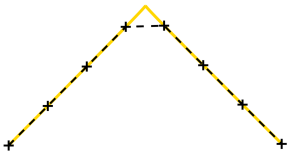

FIGURE 7. A DESIGN PROFILE (YELLOW SOLID LINE) AND THE CORRESPONDING TARGET PROFILE (BLACK DASHED LINE).

For the target profile shown in Fig. 6, the maximum bend angle for each profile is $-38.74°$ and $-37.83°$, respectively, when the number of pieces in each target profile is sufficient. The numbers of pieces of the target profiles are determined to be 1400 and 1404. The apices matrices are generated as

$$A_1 = \begin{bmatrix} 625 \\ -38.74° \end{bmatrix} \text{ and } A_2 = \begin{bmatrix} 466 \\ -37.83° \end{bmatrix}.$$

Since the sharp corners on two profiles have roughly equal bend angles, an $\mathscr{M}$-segment is used to approximate the region that

contains the sharp corner. A chain with a segment type vector $\mathbf{V} = [\mathscr{C}\ \mathscr{M}\ \mathscr{C}]$ is generated to match the same set of profiles. The segment matrix is determined to be

$$SM = \begin{bmatrix} 322 & 688 & 390 \\ 164 & 688 & 552 \end{bmatrix}.$$

Assembling the segments with revolute joints, Fig. 6b shows that the shape matching of both profiles is significantly improved by using the $\mathscr{M}$-segment to approximate the high-curvature region.

3.2 Shifting Endpoints for Closed Profiles

Although morphological outlines of a structure can be homologous, the points on the curves do not always have clear correspondences. For the purpose of improving shape matching, the endpoints of closed profiles may be shifted. As shown in Fig. 4, additional steps are taken for each target profile in a closed profile problem to seek an endpoint location that reduces the matching error. For the j^{th} profile, the endpoint is shifted using the method shown in Fig. 8, and the *SM* is optimized using the gradient-based method shown in Fig. 5. These two steps are repeated until the matching error of the j^{th} profile is minimized. The series of operations are performed on all profiles.

The detailed method for seeking a better endpoint of the j^{th} profile given a specified *SM* is as follows (Fig. 8). First, two new sets of target profiles are generated separately by shifting the endpoint location of the j^{th} profile by one piece forward (set 1) and backward (set 2) along one profile while keeping the endpoints of the other profiles unchanged. Then, segments are generated for each set of the new target profiles using the original *SM*. The average matching error of each new set of target profiles is measured and compared to the original error. If the matching error is decreased after shifting the endpoint in one direction, then the endpoint location continues to be shifted in that direction until the error stops decreasing. Thus the endpoint of the j^{th} target profile is shifted to the location where a lower matching error is obtained with the given *SM*.

For example, as shown in Fig. 9, the profiles in Fig. 2b originally have their endpoints located at (405.0, 936.0), (399.0, 896.0), and (405.5, 845.0). With a segment matrix

$$SM = \begin{bmatrix} 31 & 91 & 58 & 84 & 83 & 91 & 132 & 123 & 128 & 12 & 171 \\ 47 & 91 & 49 & 84 & 86 & 91 & 96 & 123 & 109 & 12 & 113 \\ 30 & 91 & 41 & 84 & 90 & 91 & 48 & 123 & 69 & 12 & 121 \end{bmatrix},$$

the average matching error is $\bar{E} = 7.0414$. Using the presented method, the endpoints are shifted to (410.5, 935.9) (+2 pieces), (369.5, 888.7) (-11 pieces), and (421.9, 847.7) (+6 pieces). The

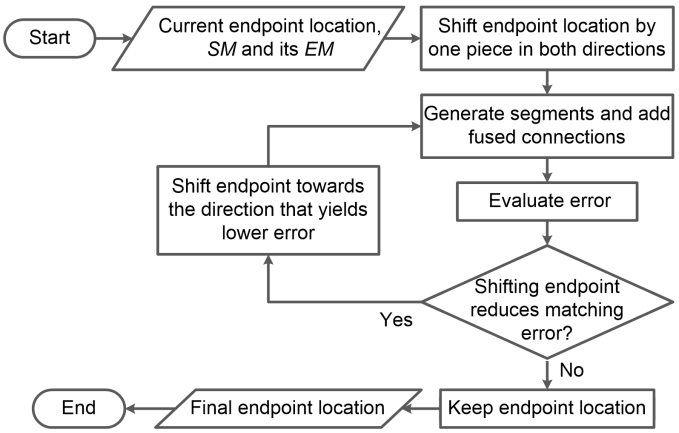

FIGURE 8. SHIFTING ENDPOINT LOCATION OF A CLOSED PROFILE WITH A GIVEN *SM* (THE STEP MARKED BY '**' IN FIG. 4).

segment matrix is also adjusted during the process and becomes

$$SM = \begin{bmatrix} 34 & 94 & 52 & 81 & 79 & 94 & 129 & 124 & 129 & 15 & 173 \\ 50 & 94 & 47 & 81 & 89 & 94 & 92 & 124 & 106 & 15 & 109 \\ 33 & 94 & 42 & 81 & 93 & 94 & 39 & 124 & 66 & 15 & 119 \end{bmatrix}.$$

The average matching error is reduced to $\bar{E} = 6.3331$ (by 10%). The final chain is presented in Fig. 13b.

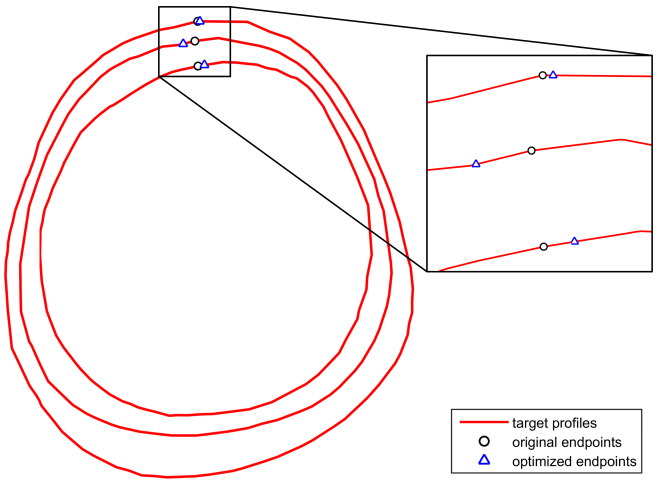

FIGURE 9. THE ENDPOINTS OF THE CLOSED PROFILES OF FIG. 2b ARE SHIFTED TO REDUCE MATCHING ERROR.

3.3 Assembling the Chain with Revolute Joints

After the geometry of all segments is determined, the final step is to add revolute joints to assemble the segments into a continuous chain. The final configuration of the chain should satisfy certain boundary conditions. Closed profiles require two endpoints of the chain to coincide with each other. Fixed-end profiles require the endpoints of the chain fixed in the designated locations. In addition, the link approximating the fixed prismatic joint of fixed-end profiles needs to remain in the same orientation. The MATLAB nonlinear programming function *fmincon* is used to solve for the final configuration of the chain with revolute joints added.

After the segments are fused and aligned with the profiles at the error-minimizing location, the current configuration is measured and the information is used as the initial guess of the final configuration. Many local minima exist in the solution field, therefore a pool of initial guesses that are slightly varied from the original values are investigated.

The function that is used to minimize the average matching error of all points on the chain is

$$f = \frac{\sum_{j=1}^{p} \sum_{i=1}^{N_j} \left\| \bar{\mathbf{z}}_j^i - \mathbf{z}_j^i \right\|}{p \sum_{j=1}^{p} N_j}, \tag{3}$$

where $\mathbf{z}_j^i$ is the position vector of the i^{th} point on the j^{th} target profile, and $\bar{\mathbf{z}}_j^i$ is the position vector of the corresponding point on the chain.

The output of *fmincon* is the coordinates and angles that defines the final configuration of the chain for all p profiles. Specifically, the output includes (i) the coordinates of the starting point of the chain, (ii) the starting orientation of the chain, (iii) the arc lengths of $\mathscr{C}$-segments, and (iv) the angles of revolute joints.

The constraints used for *fmincon* are as follows. The difference in the arc length of each $\mathscr{C}$-segment between the unconnected chain and the assembled chain is limited to 10% to preserve the current arc length and shape of the $\mathscr{C}$-segments. Boundary conditions such as the endpoint locations for fixed-end and closed profiles are also applied.

4 EXAMPLES

Three morphometric problems are investigated by applying the presented rigid-body chain methodology. The first problem is the analysis of cochlea shapes of human subjects. The second problem is the spatiotemporal evolution of human skull profiles. The third problem studies the growth of the head circumference of children. For these three very different problems, geometric morphometrics methods require the researcher to identify corresponding landmarks on each sample. Complex shapes and high numbers of samples call for a large number of landmarks, eventually leading to a long and tedious analysis task. With the presented method, the researcher only needs to specify a segment type vector and a connection type vector to analyze all the samples. The segment and connection type vectors may be determined generally (the cochleas and the skull profiles) or based on some assumptions proposed by experts (the head circumferences).

4.1 The Cochleas

The cochlea is the auditory portion of the inner ear. The length and shape of the cochlea are related not only with growth [12] and gender [13], but also with phylogenetics [14]. The cochlea has a smooth 3D spiral shape, therefore geometrical feature points are lacking. Consequently, the shape of the cochlea cannot be analyzed using any classical methods of morphometrics based on landmarks. Previous research analyzed the cochlea in terms of length, number of turns, angles, scaling, etc. [15, 16]. Some researchers tried to distribute landmarks regularly over the center line [17] which estimates quite precisely the overall shape, but the correspondence between the landmarks of different samples is arguable.

A total of 21 profile curves are collected from 10 female and 11 male children aged from 2 months to 5 years old. Each profile curve is the 2D projection of the 3D centerline of the cochlea on a common plane. Although unnecessary for the presented method, all the curve data obtained had been scaled to a roughly equal size. The segment type vector is selected to be $\mathbf{V} = [\mathscr{M}\ \mathscr{M}\ \mathscr{M}\ \mathscr{M}\ \mathscr{C}\ \mathscr{M}\ \mathscr{M}\ \mathscr{C}\ \mathscr{M}\ \mathscr{M}\ \mathscr{M}]$. All segments are connected by revolute joints. As shown in Fig. 10, a single rigid-body chain is able to fit very precisely all 21 cochlea profiles. The average width and length of the cochlea profiles are 798.68 and 976.40 respectively, while the mean matching error of the whole chain for all profiles is 6.91 (0.87% of the width and 0.71% of the length). This means that with only 12 parameters (the 10 angles of the revolute joints and the 2 centric angles of the prismatic joints), the shape of a cochlea can be defined without pointing any landmarks. This small set of parameters can be used for morphometric analysis, such as building a mean model for each gender by averaging the parameters or assessing the sexual dimorphism by contrasting the parameters among the gender groups.

4.2 Skull Profiles

Five sagittal skull profiles corresponding to different stages in human evolution were investigated: *Australopithecus*, *Homo habilis*, *Homo erectus*, *Homo neanderthalensis*, and *Homo sapiens*.[1] Unlike the smooth cochlea profiles, the sagittal skulls have complex shapes, hence the number

[1] Outline resources available at: http://www.deformetrica.org/?page_id=105

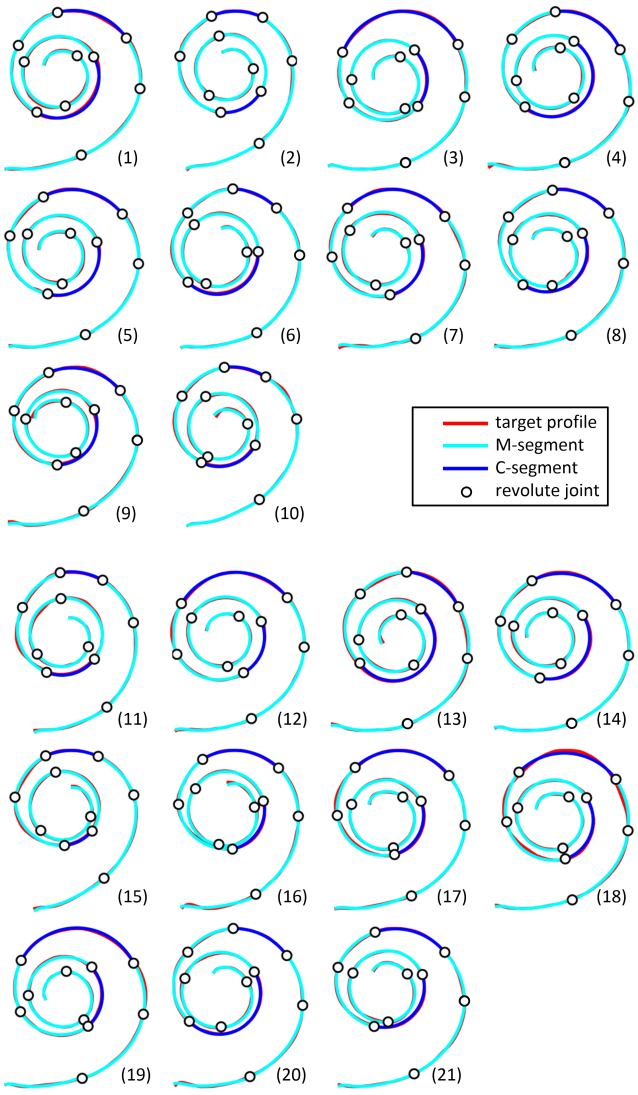

FIGURE 10. A SINGLE RIGID-BODY CHAIN MATCHES THE COCHLEA PROFILE CURVES OF 10 FEMALE INDIVIDUALS (1-10) AND 11 MALE INDIVIDUALS (11-21).

of segments contained in the chain is increased. These skull profiles are closed profiles. As shown in Fig. 11, the chain contains 51 segments, with the segment type vector $\mathbf{V} = [\mathscr{M}\ \mathscr{M}\ \mathscr{M}\ \mathscr{C}\ \mathscr{M}\ \mathscr{M}\ \mathscr{M}\ \mathscr{C}\ \ldots\ \mathscr{M}\ \mathscr{M}\ \mathscr{M}\ \mathscr{C}\ \mathscr{M}\ \mathscr{M}\ \mathscr{M}]$ (12 $\mathscr{C}$-segments and 39 $\mathscr{M}$-segments). All segments are connected by revolute joints. With an average width and length of 165.50 and 171.20 for the profiles, the mean matching error of the chain is 0.65 (0.39% of the width and 0.38% of the length). The complex shapes of the skull profiles are successfully characterized with only 63 parameters (the 51 angles of the revolute joints and the 12 centric angles of the prismatic joints) without using any landmarks. Now, in order to use the result in evolution study, the trajectory of the corresponding joints still needs to be analyzed to see if they correspond to homologous features (points which are considered as correspondent from a biological point of view) and if the parameters can help to characterize and quantify shape modifications (as receding forehead or protuberant face) along human evolution as in [18].

This case also reveals the current general strategy for determining the segment type vector $\mathbf{V}$ for complex profiles. That is, the initial $\mathbf{V}$ is composed of a sufficient number of repeating segments ($[\mathscr{M}\ \mathscr{M}\ \mathscr{M}\ \mathscr{C}]$ in the skull case). One segment or a few segments are $\mathscr{C}$-segments for the purpose of varying the chain's arc length, while the majority are $\mathscr{M}$-segments as they approximate shapes better, which is especially critical for complex profiles. During the optimization, some of the segments might be reduced to a minimum segment length (defined by their number of pieces), and these segments are eliminated from the chain. In this way, the segment type vector $\mathbf{V}$, together with the connection type vector $\mathbf{W}$, is evolved during the optimization process.

4.3 Head Circumferences

The analysis of transverse head shape as a child grows may have direct clinical applications in the case of cranial deformation as plagiocephaly [19]. The head outline of an affected child can be drawn as a closed curve. Studying the head outline over time may help to understand if the head growth becomes normal or not and evaluate the severity of the deformation or the efficacy of a therapeutic procedure. Each curve corresponds to the head circumference of a child at a given date. According to suggestions from a pediatric surgeon, the transverse skull outline of a child is symmetrical and can be divided into 5 rigid (bony) parts (2 frontal, 2 partietal, and 1 occipital) that can be modeled by $\mathscr{M}$-segments, and 5 growing parts containing the suture areas (1 metopic, 2 coronal, and 2 lambdoid) that can be modeled by $\mathscr{C}$-segments (see Fig. 12). Since the endpoint of the design profile is located at the center of forehead, the frontal $\mathscr{C}$-segment is decomposed into two fused $\mathscr{C}$-segments. To constraint the deformation of the skull, only one degree of freedom is allocated between the bony parts and the growing parts by setting a fused connection at one side of the $\mathscr{C}$-segment and a revolute joint at the other side. The segment type vector and the connection type vector are then determined to be $\mathbf{V} = [\mathscr{C}\ \mathscr{M}\ \mathscr{C}\ \mathscr{M}\ \mathscr{C}\ \mathscr{M}\ \mathscr{C}\ \mathscr{M}\ \mathscr{C}\ \mathscr{M}\ \mathscr{C}]$ and $\mathbf{W} = [\mathscr{F}\ \mathscr{F}\ \mathscr{R}\ \mathscr{F}\ \mathscr{R}\ \mathscr{F}\ \mathscr{F}\ \mathscr{R}\ \mathscr{F}\ \mathscr{R}\ \mathscr{F}]$, where the first fused connection refers to the connection between the first and the last segments. Figure 13a and b show the application of rigid-body chain matching the growth of head circumferences of two different children over three time steps. For the case in Fig. 13a, the maximum diameter of the head circumference is approximately 567.50 and the mean matching error is 2.61 (0.46% of the diameter). For the case in Fig. 13b, the maximum

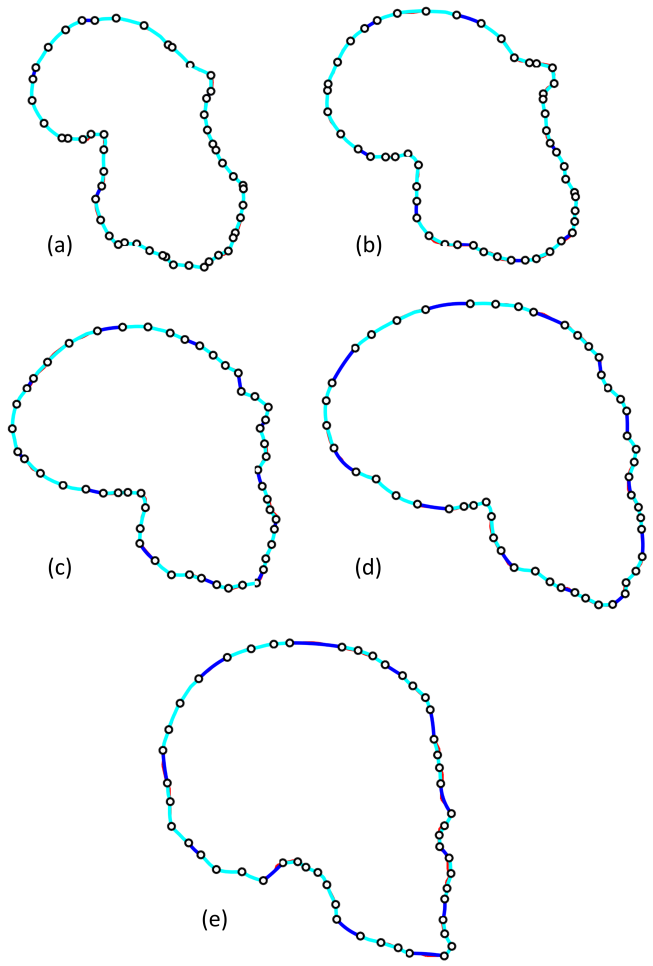

FIGURE 11. FITTING THE SAGITTAL SKULL OUTLINES OF (a) AUSTRALOPITHECUS, (b) HABILIS, (c) ERECTUS, (d) NEANDERTHALENSIS, AND (e) SAPIENS, WITH A SINGLE RIGID-BODY CHAIN.

head circumference diameter is about 877.1672, and the mean error is 6.8956 (0.79%). In both cases, the fitting is accurate with only 9 parameters (the 4 angles of the revolute joints and the 5 centric angles of the prismatic joints). This small set of values could help the physician to better keep track of the growth of the shape or the evolution of any therapy. These results also show that the mechanical structure does not only allow some constraints in the space of possible deformations, but also may be correlated to concrete hypotheses depending on the application.

5 CONCLUSION

This paper presents the developments in the methodology for synthesizing rigid-body chains for shape matching and also

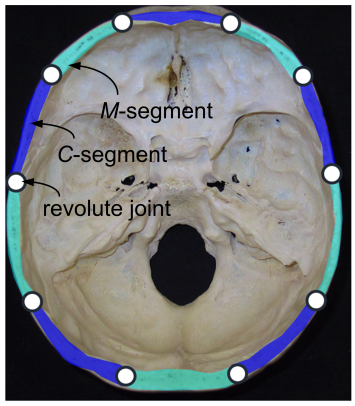

FIGURE 12. THE MECHANICAL STRUCTURE OF A TRANSVERSE SKULL BASED ON ANATOMICAL ASSUMPTIONS.

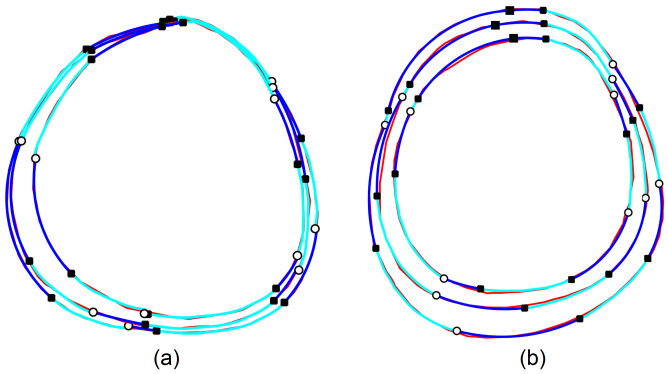

FIGURE 13. THE RESULTS OF FITTING TWO SETS OF HEAD CIRCUMFERENCE PROFILES THROUGH THREE TIME-STEPS.

applies the technique to different morphometric problems. The shapes to be matched are represented by a set of curves) which can be open or closed. The methodology generates a chain of rigid bodies connected by revolute or prismatic joints to match the set of prescribed profiles. A pool of initial segment matrices *SM* are randomly generated, among which the ones that yield the lowest error would be optimized through an iterative gradient-driven process. Constraints of the *SM* would be addressed if the profiles contain sharp corners. The endpoint would be shifted for closed profiles to reduce matching error. In the end, revolute joints are added to assemble the chain. Three morphometric problems are analyzed using the presented methodology. The results validate that the rigid-body chain technique could be employed as an alternative method for morphometrics.

6 ACKNOWLEDGMENT

This material is based upon work supported in part by the National Science Foundation under Grant No. #1234374.

Bingjue Li acknowledges the University of Dayton Office for Graduate Academic Affairs for supporting her scholarship. We also thank Jean Dumoncel (AMIS Laboratory, Toulouse, France), Stanley Durrleman (INRIA, Paris, France), Guillaume Captier and Rémy Brun (University Hospital, Montpellier, France) for giving access to curve data.

REFERENCES

[1] Adams, D. C., Rohlf, F. J., and Slice, D. E., 2004. "Geometric morphometrics: Ten years of progress following the 'revolution"'. Italian Journal of Zoology, **71**(1), pp. 5–16.

[2] Blackith, R. E., and Reyment, R. A., 1971. Multivariate Morphometrics. Academic Press, New York.

[3] Marcus, L. F., 1990. "Traditional morphometrics". In Proceedings of the Michigan morphometrics workshop, F. J. Rohlf and F. L. Bookstein, eds., University of Michigan Museum of Zoology, pp. 77–122.

[4] Ferson, S., Rohlf, F. J., and Koehn, R. K., 1985. "Measuring shape variation of two-dimensional outlines". Systematic Biology, **34**(1), pp. 59–68.

[5] Rohlf, F. J., 1986. "Relationships among eigenshape analysis, Fourier analysis, and analysis of coordinates". Mathematical Geology, **18**(8), pp. 845–854.

[6] Francuski, L., Vujić, A., Kovačević, A., Ludoški, J., and Milankov, V., 2009. "Identification of the species of the Cheilosia Variabilis group (Diptera, Syrphidae) from the Balkan Peninsula using wing geometric morphometrics, with the revision of status of C. Melanopa Redi Vujić, 1996". Contributions to Zoology, **78**(3), pp. 129–140.

[7] Murray, A. P., Schmiedeler, J. P., and Korte, B. M., 2008. "Kinematic synthesis of planar, shape-changing rigid-body mechanisms". Journal of Mechanical Design, **130**(3), p. 032302.

[8] Persinger, J. A., Schmiedeler, J. P., and Murray, A. P., 2009. "Synthesis of planar rigid-body mechanisms approximating shape changes defined by closed curves". Journal of Mechanical Design, **131**(7), p. 071006.

[9] Shamsudin, S. A., Murray, A. P., Myszka, D. H., and Schmiedeler, J. P., 2013. "Kinematic synthesis of planar, shape-changing, rigid body mechanisms for design profiles with significant differences in arc length". Mechanism and Machine Theory, **70**(0), pp. 425 – 440.

[10] Li, B., Murray, A. P., and Myszka, D. H., 2015. "Designing variable-geometry extrusion dies that utilize planar shape-changing rigid-body mechanisms". In ASME 2015 International Design Engineering Technical Conferences, Vol. 5.

[11] Zhao, K., Schmiedeler, J. P., and Murray, A. P., 2012. "Design of planar, shape-changing rigid-body mechanisms for morphing aircraft wings". Journal of Mechanisms and Robotics, **4**(4), p. 041007.

[12] Jeffery, N., and Spoor, F., 2004. "Prenatal growth and development of the modern human labyrinth". Journal of Anatomy, **204**(2), pp. 71–92.

[13] Sato, H., Sando, I., and Takahashi, H., 1991. "Sexual dimorphism and development of the human cochlea. Computer 3-D measurement". Acta Otolaryngol, **111**(6), pp. 1037–40.

[14] Braga, J., Loubes, J.-M., Descouens, D., Dumoncel, J., Thackeray, J. F., Kahn, J.-L., de Beer, F., Riberon, A., Hoffman, K., Balaresque, P., and Gilissen, E., 2015. "Disproportionate cochlear length in genus *Homo* shows a high phylogenetic signal during apes hearing evolution". PLoS ONE, **10**(6), p. e0127780.

[15] Hardy, M., 1938. "The length of the organ of corti in man". American Journal of Anatomy, **62**(2), pp. 291–311.

[16] Spoor, F., and Zonneveld, F., 1995. "Morphometry of the primate bony labyrinth: A new method based on high-resolution computed tomography". Journal of Anatomy, **186**(2), pp. 271–286.

[17] Gunz, P., Ramsier, M., Kuhrig, M., Hublin, J.-J., and Spoor, F., 2012. "The mammalian bony labyrinth reconsidered, introducing a comprehensive geometric morphometric approach". Journal of Anatomy, **220**(6), pp. 529–543.

[18] Durrleman, S., P. X. T. A. B. J. G. G., and Ayache, N., 2013. "Toward a comprehensive framework for the spatiotemporal statistical analysis of longitudinal shape data". International Journal of Computer Vision, **103**(1), pp. 22–59.

[19] Captier, G., Dessauge, D., Picot, M., Bigorre, M., Gossard, C., Ammar, J. E., and Leboucq, N., 2011. "Classification and pathogenic models of unintentional postural cranial deformities in infants: plagiocephalies and brachycephalies". Journal of Craniofacial Surgery, **22**(1), pp. 33–41.